JOURNAL OF SPACECRAFT AND ROCKETS
Vol. 48, No. 3, May–June 2011

Base Flow Studies for a Single-Engine Launch Vehicle Configuration

Tina Thomas* and C. Unnikrishnan†
Vikram Sarabhai Space Centre, Thiruvananthahpuram, 695 022, India

DOI: 10.2514/1.51401

The base-flow parameters of a single-engine launch vehicle configuration have been numerically investigated using a finite-volume-based compressible Navier–Stokes code. The axisymmetric flow simulations have been done on a structured grid for different trajectory conditions of the flight path when the engine jet is on. The freestream flow regime covers high-transonic to supersonic Mach number conditions for constant nozzle exit conditions. The interaction of the jet from the nozzle and external freestream is taken into account in the computation. The Baldwin–Lomax turbulence model is used to capture the Reynolds stresses to account for the turbulent viscosity. The distribution of pressure and heat flux in the base region, nozzle external surface, and the external surface of the base cylinder are computed. The computed pressure and heat flux values are compared with available flight measurements.

Nomenclature

D = cylinder diameter, m
d = nozzle exit diameter, m
H = altitude, km
M = Mach number
t = time, s
P = pressure, Pa
s = curvilinear distance, m
T = temperature, K

I. Introduction

ONE of the important aspects of any rocket design is that the materials used for the rocket structure should withstand the severe thermostructural loads acting on these bodies during its flight. An accurate estimate of the surface pressures and heat fluxes acting on these bodies is therefore essential for proper selection of materials and for giving optimal thermal protection system. A critical region where extreme care should be taken for the above factors is the base region of a launch vehicle, where excessive heating is a major problem to be handled, as several sensitive electronic components are housed in this region. As the launch vehicle ascends through the atmosphere into space from its sea-level launch position, the rocket exhaust plumes expand to a point where a plume reverse flow is encountered. The reverse jet impinges on base surface areas, components, and base shields, causing heating, contamination, and/or possible combustion in the launch vehicle base regions.

The base flow in launch vehicles is an extremely complex phenomenon, and it is difficult to predict the base pressures and heat flux. Generally, it is not possible to simulate all the flight parameters like the high motor chamber pressures and the high-altitude environment in an experimental setup. Again, the scaling law from the experiments to flight conditions is not readily available. The empirical approach uses a combination of data correlations and semitheoretical models like the Korst model [1]. It works well for simple configurations. However, these methods are not reliable when complex geometry and flow physics are involved. A potential alternative to the above conventional methods is computational fluid dynamics (CFD), which has none of the above restrictions and is becoming more feasible, due to maturing algorithms and advancing computer technology.

Turbulence modeling represents one of the major limitations in practical work, especially in highly compressible flows and separating flows. In fact, there is no single turbulence model that is applicable to all problems. Today, the models commonly used range from simple algebraic models like Baldwin–Lomax to two-equation models like k-ε models and to the Spalart–Allmaras model. Various studies on base flows using different turbulence models have been reported in literature. These include studies using algebraic models of Baldwin–Lomax [2–5], one-equation Baldwin–Barth model [6], and two-equation models like k-ε [7]. A comparison between algebraic and two-equation k-ε models for base flow has been done by Peace [8] for afterbody/nozzle geometries. Not all turbulence models are able to predict heat flux accurately. For example, using some of the k-ε models, it is difficult to get the gradients at the wall, which is essential for predicting heat flux. Turbulence models can also add uncertainties to the predictions. Serpico et al. [9] have studied the base flow of the Italian lightsat launcher Vega using both the algebraic and two-equation models and reported that satisfactory agreement exists between both the models.

It is seen that most of the papers reported in literature are concerned with the prediction of base pressure only. None of the references quoted above address the prediction of the base-heating problem. In the present paper an attempt has been made to compute the base-flow heating of a launch vehicle configuration for different freestream trajectory conditions when the engine is thrusting.

II. Numerical Analysis

Figure 1 shows the full configuration of a typical launch vehicle with the heat shield and the cylinder. The base region with the engine nozzle is also shown in the figure. However, for the present simulation, the heat-shield portion with the front spherical-cone region is not considered. Since the base region is located far away from the heat shield of the vehicle, the effect of the detached shock and the resulting changes in the flowfield are not likely to affect the flow in the base region, where a uniform approaching freestream can be assumed. The geometry considered for simulation, also shown in figure, consists of the base cylinder and the nozzle geometry only, which are the regions of interest in the present study.

The computations have been performed using an axisymmetric Navier–Stokes code with the objective of simulating the flow in the base region of a launch vehicle. Special emphasis is given to compute

Received 30 June 2010; revision received 19 November 2010; accepted for publication 22 November 2010.

*Engineer, Aerodynamics Research and Development Division, Aerothermal Design Group.
†Senior Engineer, Aerodynamics Research and Development Division, Aerothermal Design Group.

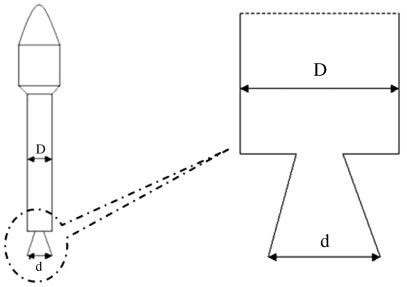

Fig. 1 Launch vehicle: full configuration and configuration considered for computations.

the heat fluxes and pressures in the base, cylinder and nozzle regions for different flight conditions when the engine is thrusting. The finite-volume-based cell-centered CFD code solves the compressible Reynolds-averaged thin-layer Navier–Stokes equations. It uses the upwinding scheme of Van Leer flux vector splitting for the inviscid convective part and central differencing for the viscous diffusive part and an implicit time integration procedure with an approximately factored bidiagonal scheme. A MUSCL-type approach is employed for the evaluation of the fluxes at the cell interfaces and a maximum of third order accuracy can be achieved in the spatial direction. The Van Albada limiter is used to avoid spurious oscillations of the solution. The implicit time integration involves using of the approximated factorization and splitting of the fluxes. By using these methods block tridiagonal equations are obtained, which can again be simplified to get block-bidiagonal equations. These block-diagonal equations are inverted using a technique similar to the MacCormack method [10]. The resulting implicit stage consists of a backward and forward sweep in every coordinate direction. The code has already been used for simulating many problems involving complex flow phenomena [11,12].

To capture the turbulent nature of the flow, the algebraic turbulence model of Baldwin–Lomax [13] is used to compute the Reynolds stresses. In the present approach, the two-layer model consisting of the inner law and outer law is used in the wall region. In the jet region, which is similar to the wake flow, the outer law is used. This model computes the turbulent viscosity to which the fluid viscosity is added to get the effective viscosity for computation. The basic assumption in this model is that the turbulent viscosity coefficient depends only on the instantaneous local flow variables. In spite of the simplicity, this zero-equation model often gives good results, compared with the more complex models like the two-equation k-ε models, as reported by the study of Serpico et al. [9]. This turbulence model requires a reference line within the computational domain for the wake flow computation. The centerline has been chosen as the reference line for this purpose, in line with the studies reported earlier using the algebraic turbulence model.

In reality, the external stream and the jet stream are two different fluids and have to be treated as a two-species problem, which will make the simulations more complex and time-consuming. In this paper, as a first step, a simple methodology is adopted to treat the problem as a single-species problem by the following assumption: the thermodynamic and transport properties such as specific heat, Prandtl number, etc., are assumed to be functions of temperature and are obtained by interpolating these properties between the external freestream and the jet exhaust temperature values [14].

Simulations are done on the flight geometry with same flight nozzle exit conditions and for similar flight trajectory conditions. Since the angle of attack is zero in flight, computations have been done for an axisymmetric case. Numerical investigation of the flowfield has been carried out for five trajectory conditions. The freestream conditions considered at different times and altitudes are given in Table 1. The nozzle exit conditions are summarized in Table 2.

Figure 2 shows the computational geometry with the boundary conditions used for the present simulations. The far-field lateral boundary is taken as 10 times the nozzle exit diameter from the wall in the radial direction, where a uniform freestream condition exists. In the axial direction, the downstream boundary is kept at 15 nozzle exit diameters away from the nozzle exit. The upstream boundary is taken at about five nozzle exit diameters ahead of the starting point of the base region. Supersonic exit conditions are imposed on the downstream boundary. Freestream conditions are prescribed at the upstream boundary. At the far boundary in the lateral direction, the freestream conditions are assumed to remain unchanged. A symmetry boundary condition is taken along the centerline of symmetry. At the nozzle exit the inlet profiles of jet values are prescribed. Along the different solid walls, the no-slip condition is imposed. The surface temperature is assumed to be 300 K, as it is the local atmospheric temperature. Conduction to the solid wall and resultant increase in the surface temperature are not considered. Thus, the assumption of 300 K surface temperature will give the cold wall heat flux and can be used for the thermal design of the base region. It is also expected that conduction to the wall will not heat up the base surface and cylinder region to alter the heat flux values to a considerable amount within this interval of flight time.

To calculate the wall quantities like pressure, and especially heat flux, it is necessary to use a structured grid, where the grids are aligned to the solid walls of the body. For the present simulations, the computational grids are generated by simple algebraic methods. Figure 3 shows the computational grid employed for the present simulations and an exploded view of the grid near the base region. It can be seen that grids are highly clustered near the solid walls, to capture the boundary layer. The distance to the center of the first cell point from the solid wall is about 12 μm, which ensures that enough grid points are within the boundary layer. Along the axial direction there are 340 points in the computational grid. Of these, 100 points are in the external cylinder region, 120 points are in the base region, and 120 points are in the downstream region. Along the radial direction there 320 points. Of these, 100 points are from the centerline to the nozzle exit, 120 points are in the base region, and 100 points are outside the base region. The y^+ values are about 2.5 for case $M = 1.042$ and about 1.0 for the high-supersonic cases.

The computations are started with the freestream conditions as the initial conditions everywhere except at the nozzle exit, where the nozzle exit conditions are imposed. Initially, a Courant–Friedrichs–Lewy (CFL) number of 0.05 with a first-order spatial discretization is used. Later, the CFL number is increased gradually to a maximum of 1.0. Finally, a second-order spatial discretization that is needed to predict wall quantities accurately is introduced.

A grid independence study is made by altering the grids in the base region to show that the number of grids in the base region taken is sufficient. Figure 4 shows the heat flux in the base region with three different grids used for the case corresponding to the freestream Mach number of 2.23. It can be seen that there are some differences

Table 1 Freestream conditions

Time t, s	Altitude H, km	Pressure P, Pa	Mach number M	Temperature T, K
40	6.72	44797.6	1.042	263.0
50	10.245	27777.5	1.28	238.4
60	14.34	14943	1.74	205.6
70	19.3	6361	2.23	203.2
80	25.4	2415.6	2.78	222.3

Table 2 Nozzle exit conditions

Properties	Values
Mach number	3.14
Pressure	90170 Pa
Temperature	1841.4 K
Specific heat ratio	1.1717
Prandtl number	0.6
Molecular weight	28.96

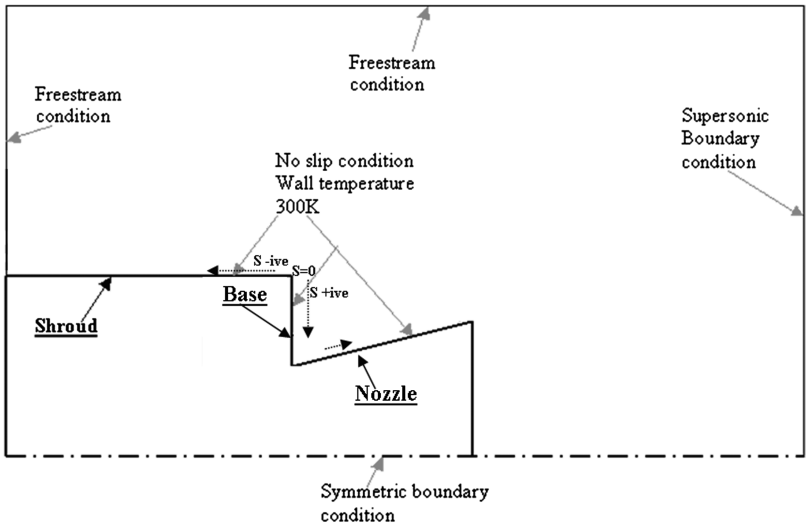

Fig. 2 Geometry with boundary conditions.

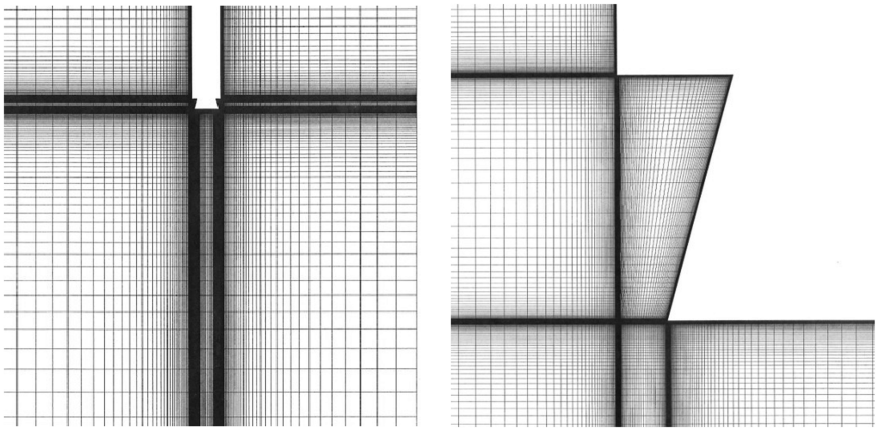

a) Full view of the grid **b) Grid near the base region**

Fig. 3 Computational grid.

between the result of 80×80 grid and 120×120 grid. But between the 120×120 grid and 150×150 grid the heat flux values are very close, showing the sufficiency of the number of grids taken. All other computations are done with the grid of 120×120 in the base region.

The convergence of the computed result for a particular simulation is shown in Fig. 5. The convergence is assumed to be reached when differences are within about 2% of the highest value between the iterations shown in the figure. The heat flux values in the base region for a typical trajectory point mentioned above are shown. Comparison made at three different iterations differing by 20,000 is shown. It can be seen that differences between the different cases are very small, ensuring the convergence of the solution. Similar convergence is also ensured for other freestream conditions.

III. Results and Discussion

As mentioned earlier, computations are done for five different trajectory conditions given in Table 1 and the results are presented. In Fig. 6, the temperature palette in the flowfield for two different trajectory conditions, corresponding to $M = 1.042$ and 2.78 are shown. The temperature shown in the palette is the nondimensional temperature with respect to nozzle exit temperature. It can be seen that for the second case ($M = 2.78$, corresponding to a higher altitude and smaller external pressure) the jet plume spreads radially outward more than for the first case ($M = 1.042$, corresponding to a lower altitude and higher external pressure). In Fig. 7, the close-up view of the Mach number palette near the base region is shown. Here, the variation is also similar to the temperature palette and is on expected lines.

In Fig. 8 the velocity vector plots corresponding to the above two cases are shown near the base region. The reverse flow towards the base region is very clearly seen in both cases. It can also be seen that for the second case (at higher altitude with lower external pressure)

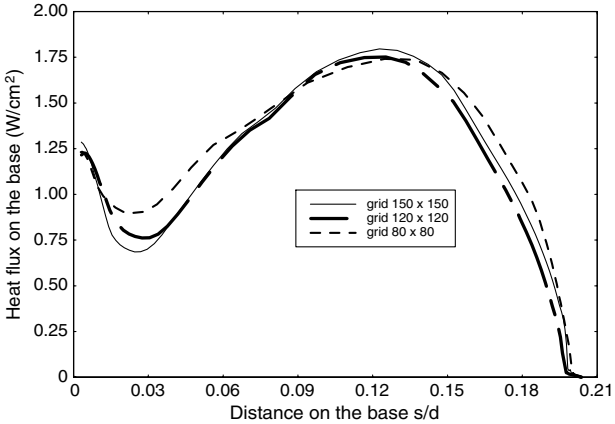

Fig. 4 Grid independence study.

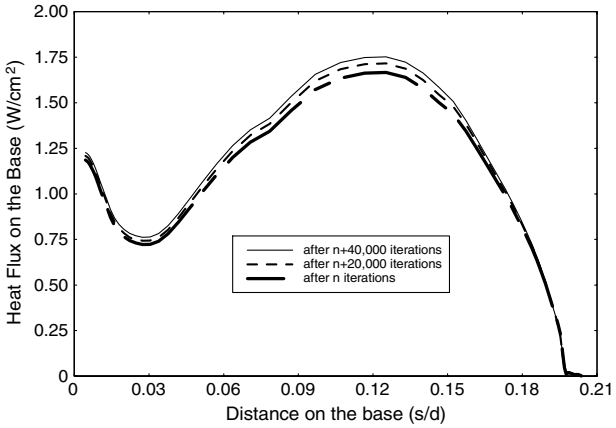

Fig. 5 Convergence of the solution.

the reverse flow is stronger than for the first case (at lower altitude with higher external pressure).

In Fig. 9, the pressure in pascals is shown for all the different cases studied along the nondimensional curvilinear length s/d of the body. The position $s/d = 0$ corresponds to the start of the base region, as shown in Fig. 2. The negative values of s/d shown are on the cylinder and the positive values are on the base region and on the nozzle external surface. From the figure it can be seen that the pressure is almost constant throughout the body surface for a particular freestream condition. It is also seen that the surface pressure is mainly decided by the freestream pressure as the surface pressures are closer to the freestream values. The surface pressure decreases with increase in Mach number and altitude, as expected, since the freestream pressure is less at the higher altitudes. The computed pressure values are compared with the measured flight pressure data. The flight data available are at a point near the center of the base region and on the cylinder ahead of the base starting point, as shown in the figure. The flight data were taken from the measurements done during the launch of a remote sensing application satellite in the year 2008. The pressure measurements were made using high-sensitivity pressure transducers with a quoted uncertainty of ± 2000 Pa. It can be seen that the comparison is very good for supersonic Mach numbers, whereas in the transonic Mach numbers, the comparison is satisfactory.

In Fig. 10 the heat flux distribution on the body surface is shown. Figure 10a shows the results for transonic Mach numbers and Fig. 10b shows the results for the supersonic freestream conditions. At lower altitude, where the Mach number is also low, the heat flux is negative on the cylinder region showing the heat flow from the surface to the fluid, where the total temperature of the fluid near the wall is less than the wall temperature. As the total temperature is lowest for $M = 1.28$, the heat flux is also lowest for this Mach number, as can be seen in the figure on the cylinder. At the base starting point there is a sudden increase in heat flux that is due to the sharp corner and the resulting sudden expansion of the flow in that

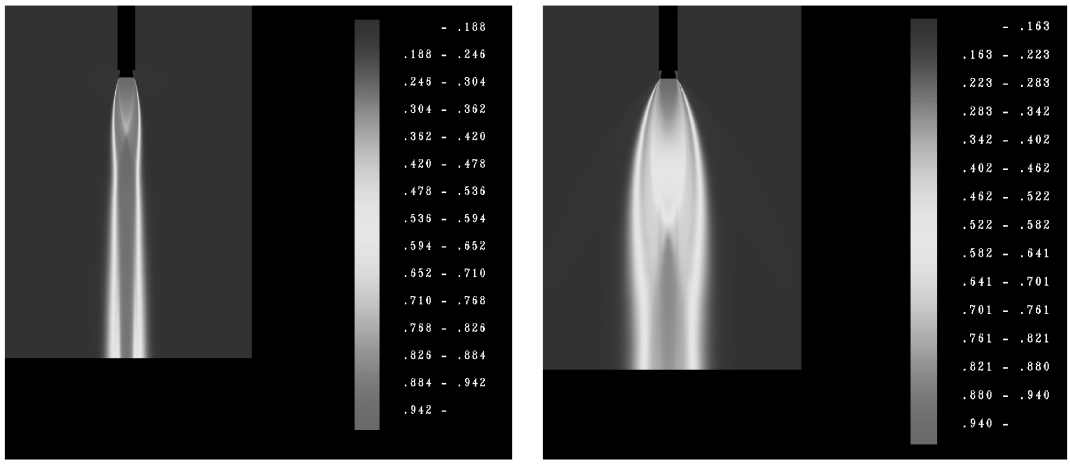

a) M= 1.042 **b) M= 2.78**

Fig. 6 Temperature palette.

a) M= 1.042 **b) M= 2.78**

Fig. 7 Mach number palette.

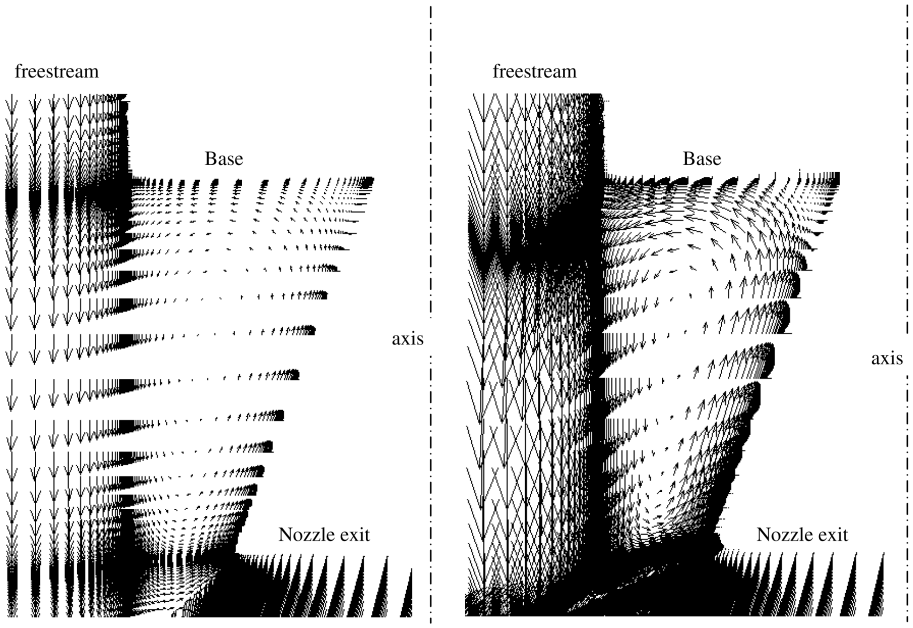

a) M= 1.042 **b) M= 2.78**

Fig. 8 Velocity vector plots near the base region.

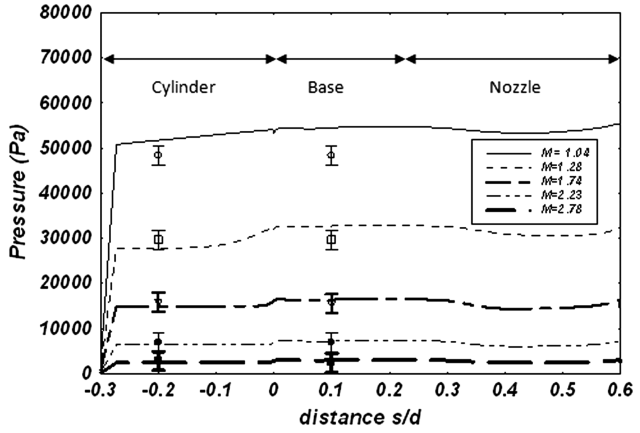

Fig. 9 Surface pressure distribution.

region. In the base region, the heat flux is maximum near the center. Near the middle of the base region, the reverse flow with higher velocity from the nozzle side directly impinges on the base portion. This could be the reason for the heat flux being highest at the center point of the base region. At the base-nozzle corner, the heat flux is nearly zero. This is due to the gases remaining virtually static at this corner. It can also be seen that at lower altitude, the heat flux is very low on the base region, indicating that the reverse flow is very weak at these lower altitudes. With increase in altitude, the reverse flow becomes strong and heat flux is also higher.

Also shown in the figures are the measured flight heat flux data obtained at almost the same points as the pressure. The heat flux measurements were made using a thin-foil-type Gardon gauge with a quoted uncertainty of ± 0.3 W/cm^2. The flight measurement values include both convective and radiative components. Initially, there is no convective component on the base region as there is no reverse flow and the measured values are radiative component only. The radiative component has been subtracted from the total to get the convective component.

It can be seen that the computed values are close to the measured values and the comparison is satisfactory considering the uncertainties in both the flight-measured values and computed values. At times 40 and 50 s, where the freestream conditions are in the transonic regime, differences between the measured data and computational results are found to be large, compared with the other trajectory conditions with supersonic freestream conditions, where a better match is observed. This discrepancy at the lower Mach numbers may be partly due to the unsteady nature of the flow in the base region resulting from the freestream transonic flow. The numerical solutions give the steady-state values at each Mach

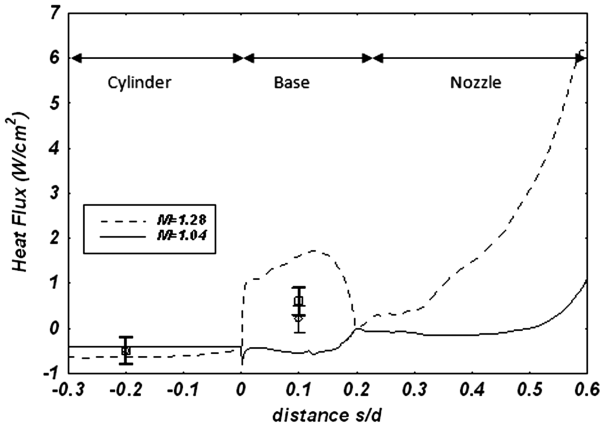

a)

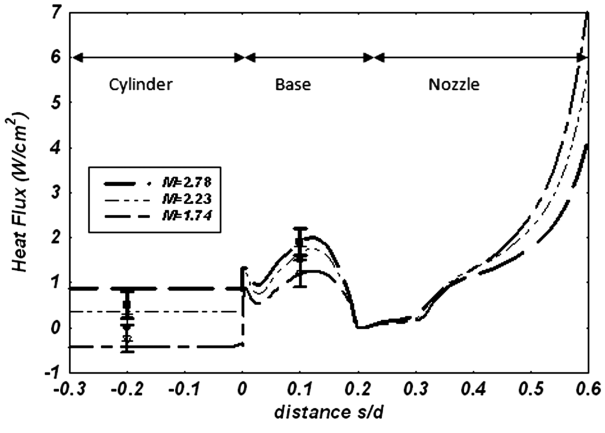

b)

Fig. 10 Heat flux distribution.

number with fully established flows in the base region. The measured values are of transient in nature, where the vehicle accelerates before the flow attains steady state. As a result, the reverse flow does not get fully established in the base region in the flight at initial Mach numbers. This can be another reason for the discrepancies at these lower Mach numbers. Considering the complexity of the problem and the uncertainties in the computation and measurements, the comparison can be considered to be satisfactory. Further studies with better turbulence models are needed to understand more about the discrepancies. A better model than the presently used simple linear interpolation method to compute the thermodynamic and transport properties of the mixture gas in the computational domain can also give better results.

IV. Conclusions

A finite-volume-based axisymmetric compressible Navier–Stokes code is used to simulate the turbulent base flow of a typical single-nozzle launch vehicle configuration with a centered propulsive jet. Simulations have been done for different trajectory conditions of the vehicle covering the high-transonic to supersonic conditions. Special emphasis is given to the heat flux computation, for which very few simulations are reported in literature. The pressure and heat flux distribution along the base region, nozzle external surface, and cylinder surfaces are given. It is found that the pressure distributions on the base region and on the nozzle external surface and cylinder are nearly constant and are mainly dictated by the external freestream pressure. The heat flux on the base region is found to have the maximum value at the center of the base region. The heat flux values on the base region and on the nozzle external surface are found to increase when the reverse flow is strong. The computed pressure and heat flux values are compared with available flight-measured data. Considering the complexities of the flow and the uncertainties in the measurement and in the simulations, the comparisons are found to be fairly good.

References

[1] Korst, H. H., "A Theory of Base Pressure in Transonic and Supersonic Flow," *Journal of Applied Mechanics*, Vol. 23, Dec. 1956, pp. 593–600.

[2] Dewert, G. S., "Supersonic Axisymmetric Flow over Boat-tails Containing a Centered Propulsive Jet," *AIAA Journal*, Vol. 22, No. 10, 1984, pp. 1358–1365.
doi:10.2514/3.48576

[3] Sahu, J., "Computations of Supersonic Flow over a Missile Afterbody Containing an Exhaust Jet," *Journal of Spacecraft and Rockets*, Vol. 24, No. 5, 1987, pp. 403–410.
doi:10.2514/3.25931

[4] Sahu, J., Nietubitz, C. J., and Steger, J. L., "Navier Stokes Computations of Projectile Base Flow with and Without Mass Injection," *AIAA Journal*, Vol. 23, No. 9, 1985, pp. 1348–1355.
doi:10.2514/3.9091

[5] Sahu, J., "Numerical Computations of Supersonic Base flow with special emphasis on Turbulence Modeling," *AIAA Journal*, Vol. 32, No. 7, 1994, pp. 1547–1549.
doi:10.2514/3.48296

[6] Hoffmann, K. A., and Suzen, Y. B., "Numerical Computation of High Speed Base Flows," 35th Aerospace Sciences Meeting & Exhibit, AIAA Paper 97-0732, Jan. 1997.

[7] Childs, R. E., and Caruso, S. C., "On the Accuracy of Turbulent Base Flow Predictions," 19th AIAA Fluid Dynamics, Plasma Dynamics and Lasers Conference, AIAA Paper 87-1439, June 1987.

[8] Peace, A. J., "Turbulent Flow Predictions for Afterbody/Nozzle Geometries Including Base Effects," *Journal of Propulsion and Power*, Vol. 7, No. 3, 1991, pp. 396–403.
doi:10.2514/3.23340

[9] Serpico, M., Schettino, A., Ciucci, A., Falconi, D., and Fabrizi, M., "Base Flow Predictions for a Lightsat Launcher at Supersonic Speeds," *Journal of Spacecraft and Rockets*, Vol. 36, No. 2, 1999, pp. 247–254.
doi:10.2514/2.3439

[10] MacCormack, R. W., "A Numerical Method for Solving the Equations of Compressible Viscous Flow," *AIAA Journal*, Vol. 20, No. 9, 1982, pp. 1275–1281.
doi:10.2514/3.51188

[11] Thomas, T. and Unnikrishnan, C., "CFD Studies for the Wing-Elevon Gap Region of a Hypersonic Re-Usable Vehicle," *11th Annual CFD Symposium*, Bangalore, India, 11–12 Aug. 2009.

[12] Jadav, B. V. S., Rasheed, H. K., and Unnikrishnan, C., "Hypersonic Wind Tunnel Diffuser Flow Analysis Using CFD," *10th Asian Symposium on Visualisation*, SRM Univ., Tamil Nadu, India, 1–5 March 2010.

[13] Baldwin, B. S., and Lomax, H., "Thin Layer Approximation and Algebraic Model for Separated Turbulent Flows," AIAA 16th Aerospace Sciences Meeting, AIAA Paper 78-257, Jan 1978.

[14] Miltion, A. B., John, L. K., and Richard, A. Y., "Jet Effects on Annular Base Pressure and Temperature in a Supersonic Stream," NASA TR R-125, 1962.

G. Palmer
Associate Editor